ENHANCEMENT OF MORPHOLOGICAL AND OPTO-ELECTRONIC PROPERTIES OF PEROVSKITE ($CH_3NH_3PbI_3$) THIN FILMS FOR SOLAR CELL APPLICATIONS.

DANIEL JUMA MORACHA [B.Ed. (Sc)]

I56/CE/28705/2015

A Thesis Submitted in Partial Fulfillment of the Requirements for the Award of a Degree of Master of Science (physics) in the School of Pure and Applied Science of Kenyatta University.

JUNE 2022

DECLARATION

This thesis is my original work and has not been presented for an award of a degree or any other award in any other university.

Signature_____date_____

Daniel Juma Moracha

I56/CE/28705/2015

Department of physics

Kenyatta University.

This thesis has been submitted for examination with our approval as the university supervisors.

Signature_____date_____

Dr. Walter Kamande Njoroge

Department of Physics

Kenyatta University

Signature_____date_____

Dr. FanuelMugwanga Keheze

Department of Physics

Pwani University.

DEDICATION

This thesis is dedicated to my dear wife Damaries, my son Dario and my beautiful daughters Duena and Paola.

ACKNOWLEDGEMENT

I want to submit my special thanks to the most high, who created the universe and all that are envisaged in it. I will always remain indebted to Him for all the good things that He has done to my life, glory be to Him. Am also grateful to my dear wife Damaries for the financial and moral support she accorded me in the entire period of my study and above all taking care of my young family in my absentia, I say a big thank you. To my friend Evans I remain grateful to you, your moral and financial support couldn't go unnoticed God bless you. My supervisors Dr. Walter Njoroge from Kenyatta University and Dr. Fanuel Kehenze from Pwani University you have been really an inspiration to me, your timely response, proper guidance made me push on even when things got tough you gave me hope. My special thanks to Pwani University administration for allowing me use their research laboratory under proper guidance from madam Mwende. I acknowledge the Physics department, university of Nairobi for making it possible for me to carry out optical and electrical measurement in their laboratory. Lastly to my course mates, material science group led by Kimutai Terer, I salute you guys.

TABLE OF CONTENTS

LIST OF FIGURES

ABBREVIATIONS

Bes	Binding energies
c-si	crystalline silicone
CdTe	cadmium telluride
DMF	N,N-Dimethylformamide
FA	Formamidinium
GaAs	Gallium arsenide
Kwh	Kilowatt-hour
LED	Light emitting diodes
MA	Methylammonium
MSSCs	Meso-superstructured Solar Cells
NA	Numerical Aperture
NREL	National Renewable Energy Labaratory
OHP	Oranometallic Halide Perovskite
OPVs	Organic photovoltaic
PCE	Power Conversion Efficiency
PHJ	PlanerHeterojuction
PL	Photoluminescence
PSCs	Perovskite Solar Cells
PV	Photovoltaic
μm	micrometer

SYMBOLS

Al_2O_3	Aluminum oxide
CH_3NH_3	Methyl ammonium
Cl^-	Chloride
Ga	Gallium
In	Indium
Pb	Lead
Te	Telluride
TiO_2	Titanium dioxide
λ	Wavelength
α	Absorption coefficient
ρ_s	Sheet resistivity
K	Extinction coefficient
Ω	Ohm
r	Radius of nucleus
g	surface free energy per unit area
I	Light intensity
S	Distance
n	Refractive index
T	Transmittance
A	Absorption
E_g	Band gap energy
E_v	Valence band
E_c	Conduction band
E_{ph}	Photon energy
E_u	Urbach energy

ABSTRACT

The functionality of the photovoltaic devices greatly depends on the film morphology, which is determined by the deposition methods and annealing techniques. Organometal halide perovskite based solar cells represents an upcoming photovoltaic technology. Perovskites have been widely and extensively studied for some years now, but comprehending their properties has slowed down their advancement. Finding a link between their morphology and the resulting properties is important in dealing with some of the basic issues like high band gap and sheet resistivity that hinder further development of this solar cell. Herein the perovskite thin films were prepared by single and double step deposition methods. Concentrations of solutions, annealing temperatures and dipping time were used as parameters to form different morphologies during self-assembly processes. The optical band gaps for the films prepared by single step were observed to decrease from 2.10eV to 1.96eV when the annealing temperature was increased from 80^{o}C to 160^{o}C. An increase of annealing temperature beyond 160^{o}C led to the formation of yellowish substance on the substrate, this indicated the presence of lead iodide. Further these results implied the decomposition of methyl ammonium which resulted to an increase of the optical band gap to 2.16eV. Films that were deposited by double step displayed similar trend where the optical band gap was observed to decrease significantly from 2.14eV to 1.95eV when the dipping time was varied from 2 hours to 8 hours. The optical band gap was observed to increase to 2.15eV when the dipping time was prolonged to 10 hours and beyond. This indicated that the nucleation and film growth of perovskite is a reversible process and 8 hours was found to be ideal for the two process to that is nucleation and film growth to perfectly take place. The transmittance data was simulated using multi-peak fitting SCOUT software from which other optical constants like refractive index was obtained as n = 2.3803, extinction coefficient k= 0.2215 and absorption coefficient α= 69855.23 for single step film samples. For the double step deposition method the refractive index of n=2.4011, extinction coefficient k= 0.2998 and absorption coefficient α= 71450.42 were revealed. The sheet resistivity of the films was evaluated using four-point probe. It was observed that an increase in annealing temperature from 80^{o}C to 160^{o}C led to decrease in sheet resistivity of films from 0.7982 Ω cm^{-1} to 0.4231Ω cm^{-1}.The sheet resistivity of films deposited by double step decreased from 0.5675Ω cm^{-1} to 0.2290Ω cm^{-1}. From the results herein it was deduced that the morphology of the perovskite thin films can be enhanced by not only the deposition methods but also annealing temperatures and dipping times.

CHAPTER ONE

INTRODUCTION

1.1 Background

Human beings are scrambling for energy as a result of development of an industrial society; this is due to the ever-increasing demand for energy by mankind and the non-renewability nature of fossil fuels. The use of these fossil fuels is a disadvantage since it is widely associated with air pollution and climate change both of which have very serious global impact and consequences. To address this researchers and scientists are looking for alternative sources of energy, which can be renewed to be used instead of fossil fuels (Guinard *et al*., 2002)

The energy from the sun is the origin of nearly all energy on planet Earth and is the most abundant of all renewable energies. As a result, developing an efficient method of harnessing solar energy would be extremely effective for satisfying the societal demand for energy (Chopra et al., 2004). Use of photovoltaic cells is one of the methods of harvesting solar energy.

The evolution of photovoltaic technology has been divided into three stages known as three generations. Silicon wafer technology represents the first generation of photovoltaic (PV), this generation is currently the one dominating the market, accounting for more than 90% of the photovoltaic market (Rathore *et al*., 2019). The raw material like polysilicon for crystalline silicon (c-si) are cheap and abundant and the devices exhibit high-power conversion efficiencies (PCE), which are typically above 25% (Zhang et al., 2015), and long-life time of about 25 years. However, these solar cells suffer from relatively high cost

for large scale production as they also require large land which may not be available. The manufacturing of solar cells also involves several toxic, flammable and explosives chemicals many of those components suppose a health hazard to workers involved in the manufacturing of solar cells.

The next stage is the second-generation solar cells. These are built on thin films with thickness of up to 1 µm (Chopra et al., 2004). This technology consists of cadmium telluride (CdTe) (Wu, 2004), copper-indium -selenide (CIS) (Guimard *et al*.,2002) and copper -indium gallium diselenide (CIGS) (Jackson *et al*., 2011). Since the solar cells are thin film this enables them to exhibit high PCE above 20%, however, owing to the scarcity of Tellurium , In, Gallium sources as well as the toxicity of heavy metals like Cadmium, solar cells are restricted to space applications and concentrator solar cells (Omondi, 2018; Fthenakis and Kim, 2007)

Third generation solar cells also referred to as emerging photovoltaic (PV) solar cells are currently under intense research and development (Jun *et al.*, 2013). Quantum dot solar cells, dye sensitized solar cells (DSSC) and organometal halide perovskite (OHP) solar cells are among the emerging photovoltaic (Andualem and Demiss, 2018).

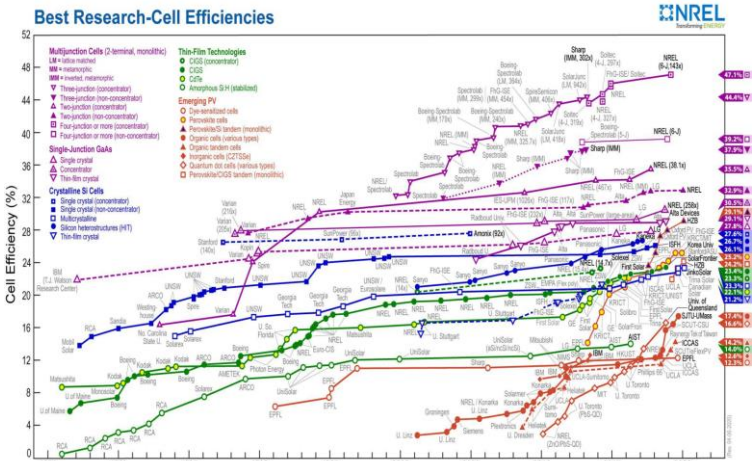

Figure 1-0-1Solar cell efficiency chart for various photovoltaic generations (National Renewable Energy Laboratory, 2021)

Solar cells made of perovskite have emerged as a reassuring technology for the upcoming third generation solar cell with a high power conversion efficiency (PCE) of above 25% as demonstrated in figure 1-0-1 above (Rao *et al*,.2016). The perovskite solar cells are desired because they are, cheap, Earth abundant, they require low temperature solution processing and high PCE as stated above. Further this material has shown a tremendous growth in terms of PCE within a short period of time. From figure 1-0-1 above, obtained from (NREL 2020) it can be clearly seen that the PCE of thin films perovskte was 14% in 2015 and within 5 year period the PCE of the said PV devices rose to 25.2% which is quite commendable. Perovskite can be represented as a block of ABX_3, where by A stands for the positive ion Methyl ammonium ($CH_3NH_3^+$), B represents an inorganic cation mostly Lead (II) ($Pb_2^{+)}$ and lastly the X_3 is a halogen anion and Chloride (Cl^-) or iodide (I^-) ions are commonly used (Park, 2015). Its structure is similar to that of calcium titanium oxide structure (Park, 2015; Leyden *et al*., 2014). This is illustrated in the figure 1-0-2 below.

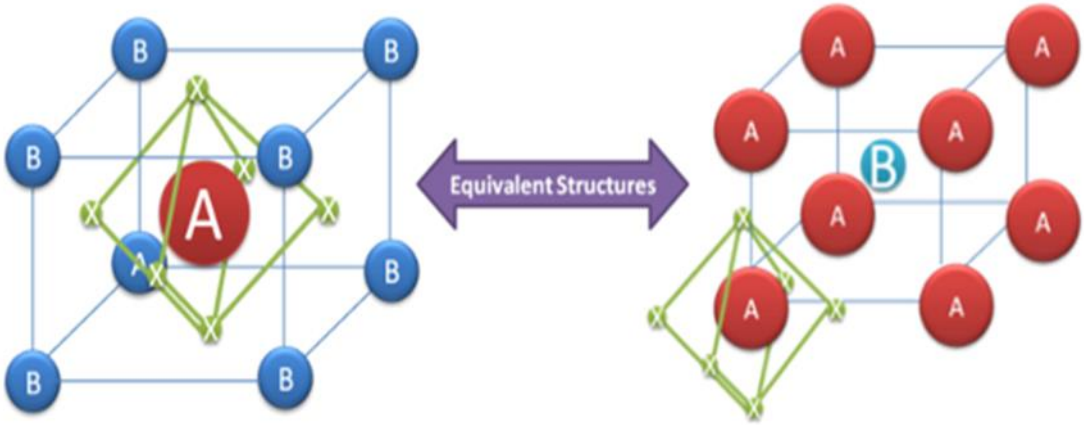

Figure 1-0-2 Schematic diagram for perovskite structure (Jena *et al*., 2019)

Recently, research on perovskite has suggested that they are good candidates to be used in solar cells (Malinkiewicz *et al*., 2014). Perovskite materials are readily available naturally, low temperature production method, cheap processing methods and their spontaneous crystalline structure organization makes the material attractive for PV devices (Fan *et al*., 2014). Given the increasing variety of materials and the sophistication of optoelectronic applications, gaining a deeper and more systematic quantitative picture of the optical and electrical properties of perovskites is important. Many researchers have therefore mainly concentrated on the structural and the opto-electronic property of perovskites. Perovskites mainly focus on both inorganic and organic characteristics of semiconductors. The simplicity of the thin film preparation methods of the perovskites makes the material attractive, but simple as it may be, it gives the material different morphologies and characteristics (Brittman *et al*.,2015).

The morphologies of the resulting crystals and films grown from solution depend critically on the choice of solvent(s), mode of their deposition, and also on substrate's morphology

and surface chemistry (Eperon *et al.*, 2014). The hybrid organic–inorganic methyl ammonium lead halide perovskites, pioneered by Mitzi, are recognized for their excellent semiconducting properties (Kagan *et al.*, 1999). From the first work of Miyasaka *et al*., (2009) these hybrid perovskite materials can be manufactured from solutions with simplicity and that makes them more attractive for photovoltaic uses (Snaith, 2013).

1.2 Problem statement

Inadequate generation and supply of low cost and environmentally sustainable energy has led to emergence of need for development of clean sources of power. Solar photovoltaic technology promises solutions to these problems, as the generation of power from solar cells is a relatively pollution free process. Over years, progressive developments in solar photovoltaic technology have taken place with much attention currently given to organic materials. Perovskites have been widely and extensively studied for some years now, but comprehending their properties has posed main challenge. Finding a link between their morphology and the resulting optical and electrical properties is important in dealing with some of the basic issues such as high sheet resistivity and large optical band gap that hinder further development thin film technology.

This study was therefore aimed at investigating the effect deposition methods and other annealing parameters like temperature and dipping time on the morphology and the effect that has on the optical and electrical properties of the resulting films.

1.3 Objectives

1.3.1 General objectives

The main objective of this study was to investigate the effects of changes in morphology on optical and electrical properties of self-assembled organometallic halide perovskite thin films formed by single-step and two-step deposition methods.

1.3.2 Specific objectives

i) Depositing perovskite thin films by single-step and double-step solution deposition methods at different temperatures and dipping times.

ii) To observe the impact of annealing temperature and dipping times on the morphologies using the optical microscopy.

iii) Determining the optical properties of $CH_3NH_3PbI_3$ films using a UV-Vis spectrophotometer

iv) Measuring the sheet resistivity of $CH_3NH_3PbI_3$ films using four-point probe set up

1.4 Rationale of the study

Organic photovoltaic technology has been lagging in terms of efficiency, and this has been a challenge to material scientists. Various studies have achieved some improvements in terms of performance of inorganic photovoltaic devices as opposed to organic PV devices. Recently organometal halide materials have attracted much attention though challenges have been met. This study thus attempted to address the challenges like high sheet resistivity and high optical band gap resulting from varying deposition methods, disordered morphology with the view of enhancing the morphology of organometal halide perovskite

thus reducing both the sheet resistivity and optical band gap making the material attractive for PV applications.

CHAPTER TWO

LITERATURE REVIEW

2.1 History of Photovoltaics

The discovery of photovoltaics dates back to 1839 when Alexandre Edmond Becquerel, French physicist, observed a weak-conducting solution and observed that a voltage appeared on one of two electrodes when illuminated (Fraas, 2014). The effects of solidified selenium on a PV were observed by Adams and Day in 1877 (Urbach, 1953). In 1904 Hallwachs used copper oxide and copper to make solar cell based on metal semi-conductor-junction. Nevertheless, this was a period of discovery since there was no comprehension of science about the devices of the first PVs operation. In 1905 Albert Einstein published an article in which he explained the photoelectric effect with assumption that light energy is being carried with quantized packages of energy (Othman and Rushdi, 2014), which are known today as photons.

In 1918 Jan Czochralski, a Polish chemist invented a procedure to grow high-quality crystalline materials. This method nowadays, is very important during the fabrication of silicon based solar cells. In 1953, American chemist Dan Trivich was the first one to perform theoretical calculations on the solar cell performance for materials with different band gaps. The real development of solar cells as we know them today, started at the Bell Laboratories in the United States in 1954 (Mitzi *et al., 2001)*. Researchers in this laboratory made a silicon-based solar cell with an efficiency of less than 5% (Green, 2009). Delaware University in 1980, achieved a PCE of above 10% when they first fabricated solar cell using the thin films of cadmium-sulfide at the junction. In 1991 Michael Grätzel and

coworkers published the first high efficiency Dye-sensitized solar cell (O'Regan and Gratzel, 1991). The Dye-sensitized solar cell is a kind of photo-electrochemical system, in which a semiconductor material based on molecular sensitizers is placed between a photo-anode and an electrolyte.

Across the years, there has been a remarkable improvement in the efficiencies of PV technologies and their deployment. For instance, traditional solar cells constructed using single-crystal silicon have yielded efficiency of up to 25.2% (Yaghoobi Nia *et al.*, 2019). Those built using gallium arsenide (GaAs) single crystals, which are considerably more expensive, have recorded efficiency of roughly 29% and 40% in single and multi-junction devices, respectively (Green *et al.*, 2015). Over time, PV technologies based on thin-film polycrystalline materials, for example, cadmium telluride (CdTe) (Baines *et al.*, 2018) and copper indium gallium selenide (CIGS) (Mohan and Paulose, 2019), emerged as a potential alternative to silicon-based cells with efficiencies > 20% (Green *et al.*, 2015). These developments led to the arrival of "third generation solar cells" (Yan and Saunders, 2014) or "emerging photovoltaics" (Parisi *et al.*, 2014), which are designed to ensure significant cost reduction of the module manufacturing and widen the applications of devices to compete with other systems of energy production. In particular, organic (Liu *et al.*, 2014) nano- and meso-structured solar cells (e.g. dye-sensitized solar cells (Chawla and Tripathi, 2015; Mathew *et al.,* 2014) and quantum dot solar cells (Chebrolu and Kim, 2019; Pan *et al.,* 2018) have been the subject of attention due to their low cost active layer materials and substrates, easy potential scalability (García-Valverde *et al.*, 2010) and simplicity of design (Kamat, 2013). After two decades of research however, and despite achieving up to 13%

efficiency, these cells did not reach mass production (Patwardhan *et al.*, 2015), due to concerns over their long term performance.

In recent years, the emergence of PV technologies based on organometal halide perovskites (Zhao and Zhu, 2014), has reinvigorated the race to develop low cost, high efficiency solar cells.

2.2 Origin of Perovskites

A new calcium titanate-based mineral was discovered in the Ural Mountains, by a German scientist by the name Gustav Rose, on his trip to Russia in 1839 (Park *et al*., 2013). This is where the origin of perovskite materials can be traced back. This new calcium titanate was named "Perovskite" in honour of this Russian mineralogist Lev von Perovski. The optical and electronic properties of perovskites was investigated by (Miyata *et al.*, 2015). In their research, they found out that the materials displayed strong exciton properties and further suggested that material was a good candidate for solar cells, transistors and light emitting diodes. However device instability posed a challenge when applied in the said PV devices. Miyasaka *et al.*, (2009) first saw the photovoltaic phenomenon in the perovskite material and used it as a sensitizer in a DSSC. The liquid sensitizers used were $MAPbI_3$ and $MAPbBr_3$ (where MA stands for CH_3NH_3), where PCE of 3.81% and 3.2% respectively, were attained by the solar cell. Nevertheless, the presence of liquid electrolyte made the device to work for few seconds due its instability.

After years of active research, they have emerged as the solar cell types with the steepest learning curve for instance some of the initial learning difficulties were device instability and achieving higher PCE but today, PCEs of above to 25% have been achieved (Green *et al.*, 2020). Requirement of simple bulk chemicals and cheaply available equipment of convectional processing (Espinosa *et al.*, 2015) eases fabrications which make this process unusual. In addition, the report from (Park, 2013) indicated that in the future, considerable efficiencies above 20% could be attained owing to perovskite thin films capacity that are coated on a mesoscopic oxide film to deliver photo voltages that are significantly higher than semiconductor quantum dots (Kamat, 2013). These characteristics offer a competitive edge in the development of devices that are commercially viable (Bisquert, 2013). Currently, with recent improvements in materials design and device architecture PCEs above 20% are routinely reported (Park *et al.*, 2016; Saliba *et al.*, 2016).

Im *et al., (*2011) used methylammonium lead iodide and achieved a PCE of 6.5% for 3.6 μm thickness of TiO_2 film. An absorption coefficient of perovskite was found to be 10 times better as compared to conventional ruthenium-based molecular dye. Park (2013) manufactured a solid-state mesoscopic organometal halide sensitized solar cell and improved the PCE to 9.7% the device experienced high degradability. Snaith (2013) made steady progress when he blended mesoporous alumina scaffold with methyl ammonium lead iodide to manufacture meso-superstructured solar cells (MSSCs) achieving 10.9% PCE. Later on, they removed the mesoporous layer and made planer heterojuction (PHJ) solar cell achieving a PCE of 15.4% however the performance of these devices was characterized by instability and high degradability.

(Lee *et al.*, 2012) demonstrated that when perovskite was used in the pores Al_2O_3 photo-anode, it performed both as light absorber and electron conductor. Etgar *et al*., (2012) made finding that organometal halide can perform as efficient hole conductor. When perovskite was deposited by novel sequential deposition technique on pores of TiO_2 film, solar cells achieved 15% efficiency Burschka *et al.*, (2013). Malinkiewicz *et al.*, (2014) came up with an inverted solar cell in which $CH_3NH_3PbI_3$ layer was placed in the middle of thin layers of electron and hole blocking that was made up of organic molecules. Deposition of organic material was done using solution based processes, while thermal evaporation and vacuum processes were used to deposit methyl ammonium lead iodide together with the metal contact. PCE of 12% was attained for these simple devices that were made under room temperature and free from metal oxide, although the efficiency of the cell was still low.

CHAPTER THREE

THEORETICAL FRAMEWORK

3.1 General Physics description of perovskites

Perovskites have a general formula of ABX_3 (X= halogen), with A and B having 12 and 6 coordinates with X anions respectively. The stability and distortion of the perovskite structure depend on the ratio of the (A-X) distance to the (B-X) distance, known as the Goldschmidt tolerance factor (equation 3.1) (Etgar *et al.*, 2016)

$$t = \frac{r_A + r_X}{\sqrt{2}(r_B + r_X)} \tag{3.1}$$

Where the denotation of the radii of an ion of A, B and X are r_A, r_B and r_x, respectively while t is Goldschmidt tolerance factor. Empirically, for the majority stable perovskite, t matches up with the values amid 0.8 and 1. If t is greater than one the site caption is too high while when t is less than 0.8, the site caption is merely small hence no formation of the perovskite structure (Brehem *et al.*, 2014).

3.2 Nucleation and crystal growth

The growth of any nuclei begins from a nucleus to a crystal seed, it takes place when a state in which the atomic particles are almost sufficient close to each other at a temperature less than the melting point. Consequently a planned arrangement of these atoms is energetically preferred (Kamat. 2013). When temperature is lowered below melting point, growth can occur from many centers of nucleus that didn't break down during the melting process. The surface apprehensions of an arithmetically created nucleus supports in growth

by maintenance atoms with the nucleus. Interchange flanked by volume and surface energy explains a decisive size higher than the regular growth begins.

Nucleation and crystal growth are two basic processes that define Perovskite formation. The supersaturation of the predecessor of solution activates nucleation of particles. A nucleus is considered as a globe condensed phase, and its liberated energy is defined by thermodynamic terms in the classical theory of nucleation (Chebrolu *et al.,* 2020). The definition of liberated energy of nucleus is given as;

$$\Delta G(r) = 4\pi r^2\gamma + \frac{4}{3}r^3\,\Delta G_v \tag{3.2}$$

And these inputs are defined as; r noted as the radius of the nucleus, γ (gamma) is the surface liberated energy per entity area and ΔG_V is the liberated energy per entity volume of a crystal. ΔG_V is described by the distinction amongst free energy of the monomer in crystal and solution. ΔG_V is prearranged as shown below

$$\Delta G_v = -\frac{RTIns}{V_m} \tag{3.3}$$

Where V_m is equivalent to the molar volume of the monomer volume in crystal. Obtaining the surface liberated energy($4\pi r^2\gamma$, positive) and mass liberated energy ($\frac{4}{3}\pi r^3\Delta G_V$, negative) keen on concern, ΔG_V is plotted.

3.2.1 Growth habit

A micro crystallite is created and well-ordered nucleus is achieved when the transportation to the surface is at a lesser speed than the diffusion across the surface. A single crystal will be formed when growth happens from a solitary seed. Polycrystalline results from statistically formed nucleus. When diffusion velocity is exceeded by the transportation, particles create amorphous solid since they lack time to find their ordered state position and more arriving atoms block the movement of these atoms hence they freeze in a highly disordered state. When atomic building blocks are larger molecules and or covalent forces leads to the easy formation of this growth (Kamat. 2013).

3.3 Optical and electrical properties

Perovskite materials have exhibited good opto-electronic properties and desirable characteristics such as low resistivity, low band gap, high electrical conductivity and high absorption coefficient, all of which are attractive for photovoltaic applications (Wehrenfenning *et al.*,2014). Organometal halide perovskite has shown vast absorption spectrum in the wavelength ranging 300-800nm, for wavelength range of less than 600nm the optical absorption coefficient is large (Yin *et al.*, 2014). The optical absorption coefficient of organometal halide perovskite is similar to common semi-conductors such as gallium arsenide (GaAs) and Cadmium telluride (CdTe) (Frost *et al.*, 2014). Perovskite are made attractive by huge absorption coefficient for wide wavelength range thus increasing its efficiency in absorbing incident light while the thickness of the absorber layer is kept minimum. It is very essential to be familiar with the elemental properties of these materials for the intend of advanced applications and the improvement of correct

systematic molds and replications. From the analysis of empirical studies it can be realized that little has been done so far to relate the morphology, optical and electrical properties of perovskite thin films deposited by single-step and double-step film preparation techniques. This study will hence establish the morphologies formed optical and electrical properties of perovskite thin films when deposited using techniques listed above.

3.3.1 Absorption of incident photons

When photons from incident radiation are absorbed, they are converted to solar power. The level of absorption of the absorber film relies on the measurable energy and energy states of every photon. Electrons from lower energy level can move to higher level when excited by an absorbed photon. The energy states in any material can be measured. Therefore, the excited electron must be given adequate energy by the incident photon for it to move to higher energy level. Transmittance of a photon through a material means the insufficiency of enough energy in a photon to eject an electron from valence band. Double-energy states arrangement is required as the bare minimum for photon energy to be absorbed, and to utilize the energy the lifespan of the carrier at the electrified state should be higher than the time needed to shift carrier from bottom energy level to higher energy level (Baines *et al*., 2018). There exists an energy gap known as the band gap energy of a material which is in-between the lower and higher energy states. The bottom energy state is known as the valence band while the higher energy state is called conduction band, an electron can move to higher conduction band in a material for double level arrangement if the photon absorbed is equal or higher than the band gap energy. There are two ways in which this can happen in semiconductor material; band-band transition as illustrated in figure 3-0-1 or defect

assisted as depicted in figure 3-0-2. Figure 3-0-1 illustrates a scenario where the photon energy is greater than the band gap energy and in this case the electron gets excited and jumps from the valence band to the conduction band before undergoing relaxation process and finally settling in the conduction band, while in figure 3-0-2 the photon energy is less than the band gap energy, in this case the energy will be absorbed by the electron but it will not be sufficient to dislodge the electron and make it move from the valence band to conduction band. This situation is rectified by doping the semiconductor with impurities what is referred in the figure as mid-gap states to aid in the movement of electrons from the valence band to conduction band (Park *et al*., 2013)

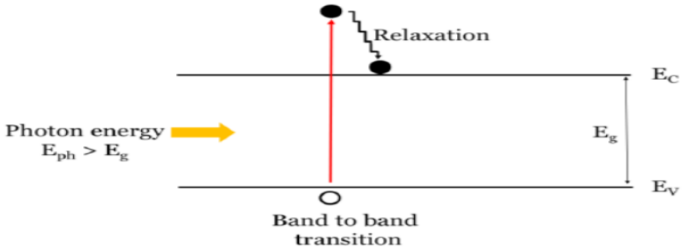

Figure 3-0-1 Band-Band transitions (Park *et al*., 2013)

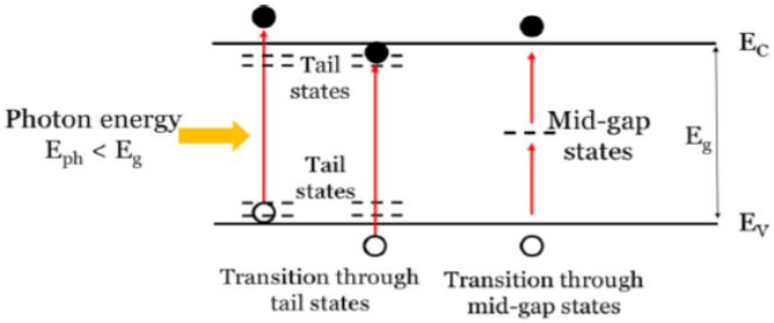

Figure 3-0-2 Defects assisted transitions (Park *et al*., 2013)

Figure3-0-3 (a) exhibits the absorption through band-band changeover when the band gap is bigger than the energy of incident photon. If the band gap is smaller as compared to photon energy an electron can transfer to level greater than the conduction band prior to slackening procedure that dispels surplus energy (hv-E_g) as heat.

Figure 3-0-3 (b) graphically shows the absorption assisted by indirect transition. This scenario can only occur if band gap is bigger than the photon energy. Solar cell loss mechanism can only occur if the band-band transition cannot be supported by the incident photon, but rather passes through a material. There are two categories of band to band transition: the indirect and direct.

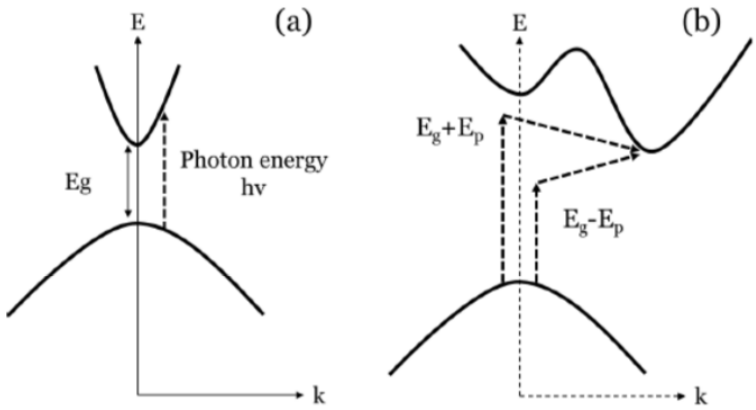

Figure 3-0-3 (a) Direct transition (b) indirect transitions (Park *et al*., 2013)

The speed of electrons and holes is constant in the valence and conduction bands while energy changes when electrons move from a state of lower energy to a state of higher energy for a direct transition, while both momentum and energy changes for indirect transition. Semiconductor material can be categorized into two: indirect and direct band gap depending on allowed transitions. A direct band gap material allows direct transmission of electrons from valence band to conduction band. An indirect band gap

semiconductor material only allows transmission of electrons if there is a change in momentum and energy. PV devices uses both direct and indirect band gap as an absorber layer.

The absorption coefficient defines quality of good absorber layer which is dependent on the wavelength of incident photon. For direct band gap semiconductors, the absorption coefficient is given by (Bost and Mahan, 1988).

$$\alpha = A\left(h\nu - E_g\right)^{\frac{1}{2}} \tag{3.4}$$

Where A is a constant and measures the disorder of the material. The higher the constant A the higher the structural disorder.

The absorption coefficient of an indirect band gap semiconductor material with an involvement of photon absorption is given by (Bost and Mahan, 1988),

$$\alpha = \frac{A\left(h\nu - E_g + E_{ph}\right)^2}{e^{\frac{E_{ph}}{kT}} - 1} \tag{3.5}$$

The effective electron and hole masses are function of A which is a proportional constant in the above equation, while hν is the energy of the incident photon, E_g is the band gap energy, E_{ph} is the photon energy being absorbed and KT is scale factor for energy values in molecular scales or simply the amount of heat required to increase the thermodynamic entropy of a system by k.

The absorption coefficients of tail and mid-gap states that are characterized by low density are related with this minimal transition. However the information of the sub-gap states distribution is relayed. The absorption coefficient of tail and mid-gap states is given by (Urbach, 1953).

$$\alpha = Ae^{\frac{hv}{E_u}} \tag{3.6}$$

E_u= Urbach energy, which is a function of tail and mid-gap defect states' distribution. Urbach energy is a parameter typically denoted, with dimensions of energy, used to quantify energetic disorder in the band edges of semiconductor. They indicate the degree of crystalline in the structure

When light transverses through a material its intensity reduces exponentially in relation to the distance travelled, which is given by the expression,

$$I = I_o e^{-\alpha s} \tag{3.7}$$

where, s is the distance, $I_o$is the intensity prior to absorption, I is the intensity and α is the absorption coefficient. For semiconductor with known thickness, the formula above can be used to calculate the amount of light absorbed.

Different semiconductor materials have different absorption coefficients. Materials with higher absorption coefficients more readily absorb photons, which excite electrons into the

conduction band. Knowing the absorption coefficients of materials aids engineers in determining which material to use in their solar cell designs (Christian and shamarr, 2019).

The absorption coefficient determines how far into a material light of a particular wavelength can penetrate before it is absorbed. In a material with a low absorption coefficient, light is only poorly absorbed, and if the material is thin enough, it will appear transparent to that wavelength. The absorption coefficient depends on the material and also on the wavelength of light which is being absorbed. Semiconductor materials have a sharp edge in their absorption coefficient, since light which has energy below the band gap does not have sufficient energy to excite an electron into the conduction band from the valence band. Consequently, this light is not absorbed. The absorption coefficient for several semiconductor materials is shown below.

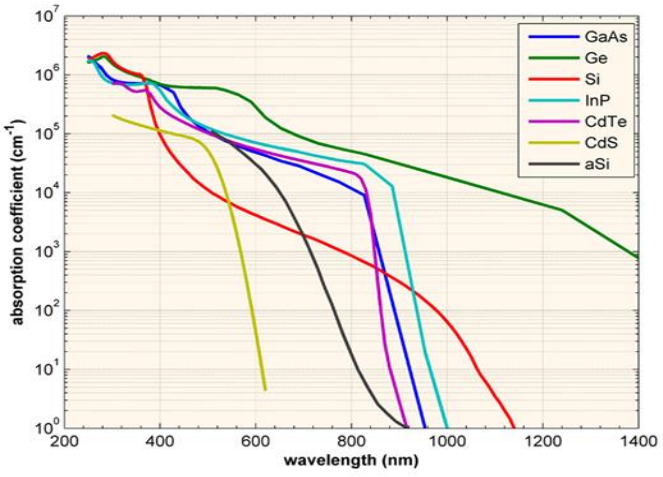

Figure 3-0-4 Absorption coefficient for various semiconductor (Christian and Shamarr, 2019)

The above graph shows that even for those photons which have energy above the band gap, the absorption coefficient is not constant, but still depends strongly on wavelength. The probability of absorbing a photon depends on the likelihood of having a photon and an electron interact in such a way as to move from one energy band to another. For photons which have energy very close to that of the band gap, the absorption is relatively low since only those electrons directly at the valence band edge can interact with the photon to cause absorption. As the photon energy increases, not just the electrons already having energy close to that of the band gap can interact with the photon. Therefore, a larger number of electrons can interact with the photon and result in the photon being absorbed. The absorption coefficient, α, is related to the extinction coefficient, k, by the following formula:

$$\alpha = \frac{4\pi k}{\lambda} \tag{3.8}$$

Where λ is the wavelength.

3.4 Optical microscope

Figure 3-0-5 shows an optical microscope with a simplified path wave. Magnification of X1500 and a 0.2 m spatial resolution can be achieved using an optical modern microscope. Microscopes can be categorized into two, namely; transmission microscope, where light passes through a transparent material and reflection microscope which reflects light that is installed on top of microscope where an opaque object is illuminated by lens. We also have observational microscopes which include; polarized light microscopes, bright field

microscopes, dark field microscopes, phase difference microscopes, interference microscopes, and fluorescent microscopes.

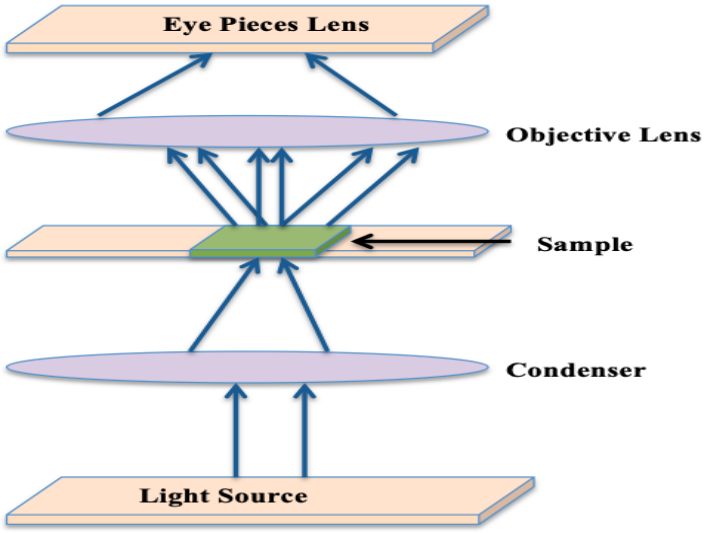

Figure 3-0-5 Schematic of the optical path of the microscope

The objective lens plays big role in determining the spatial resolution of a good microscope. The resolution power of any microscope cannot be interfered with by the eyepiece, even though it can adjust the magnification of the image. Rayleigh equation can be used to determine the spatial resolution of an optical microscope.

$$\Delta r_0 = \frac{1.22\lambda}{2n\sin\theta} = \frac{0.61\lambda}{nsin\theta} \tag{3.9}$$

The source of light wavelength is given by λ, minimum resolvable distanceΔr_0, n refractive index, $sin\theta$ half-angle aperture. The factor 1.22 comes from the definition of Bessel

function of 1st kind, the fact that the 1st minima of the diffraction pattern appears at 1.22 units from the central zero.

3.4.1 Dark field microscopy

Figure 3-0-6 below illustrates dark filed microscopy, with the specimen illuminated by oblique rays. This is made possible if the central rays that pass around the specimen are blocked. This is the most popular way of imaging specimens that are unstained which are in dark background but they are brightly illuminated. When the specimens are struck by oblique rays originating from dark field condenser they are refracted, diffracted or reflected into the objective of microscope. Dark field microscope can also be used to evaluate objects that strongly scatter light. The basic operation of dark field microscope is that the specimen is illuminated by light at an angle very high such that the light that is not deviated is not captured by the microscope objective. This is made possible when the illuminating light from the central part is blocked as shown.

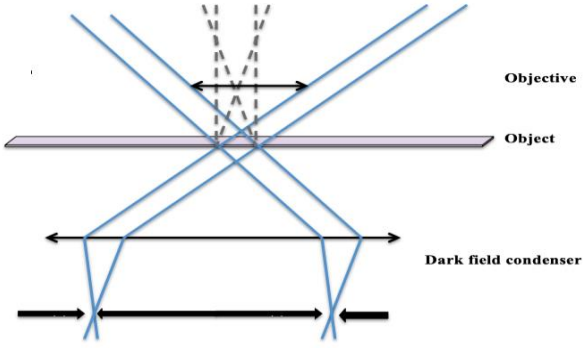

Figure 3-0-6 Illustration of dark field microscope

Polarized light microscopy

When the refractive index is the same in all directions all over the crystal lattice, the transparent material is called isotropic. The classification of crystals into isotropic or anisotropic is done majorly depending on the optical bearing or the equivalence crystal axes. When the axes are equal and the interaction of light is the same irrespective of the inclination of the crystal in relation to the incoming light the material is called isotropic. This incoming light is refracted at fixed angle and travels at undivided velocity without being affected by electronic elements of the crystal. For anisotropic the axes are different while its interaction with light heavily depends on the inclination of the crystal lattice with the incoming light. The behavior of light in anisotropic is the same as that in isotropic. But when light enters the unequal axis it is refracted at orthogonal, this gives rise to rays that travel at distinct velocities while each ray is contrasted.

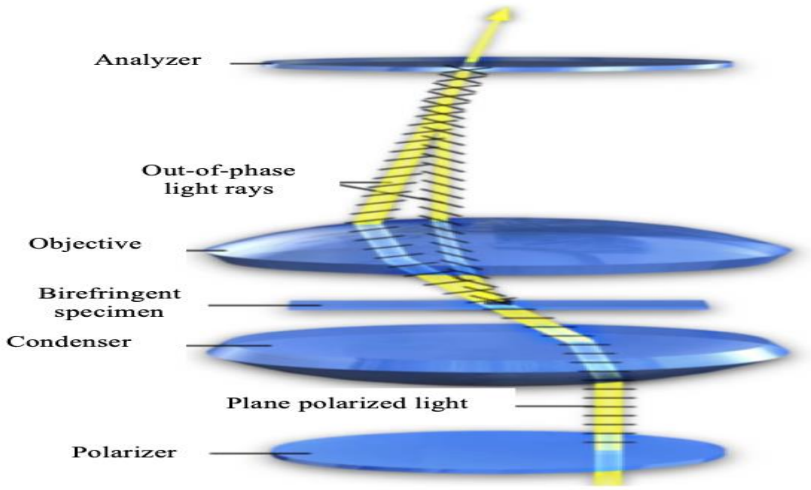

Figure 3-0-7 Polarized microscope (Michael and Mortima, 2016)

3.5 SCOUT Simulation

Theoretical analysis of experimental optical data was simulated in the scout software to obtain optical invariants of thin layers using various dielectric models in particular OJL model and Drude model were used. The OJL model was used to obtain the optical band gap by use of the gap energy E_o. When the gap energy was divided by constant value 8085 the values of the optical band gap for films annealed at different temperatures and dipping times were obtained. The Drude model was used for optical constant analysis, where constants like absorption coefficient α, extinction coefficient k and refractive index n were obtained.

3.5.1 OJL model

The O'Leary-Johnson-Lim (OJL) model is used to describe the inter-band transition in semiconductor materials. The inter-band transitions are depicted by the model that assumes the parabolic shape of the density of state (DOS) function for the valence and the conduction bands with tail states exponentially decaying into the band gap. The shape of the conduction and valence band DOS are mathematically defined as a function of energy, predominantly by the parameters E_o (defining the gap between the band edges), mass (a scaling factor determining the shape of the DOS) and gamma (reflecting the width of the exponential band tails) (El-Amin and Solieman, 2015). The fit parameters of the OJL interband transition model are the gap energy, E_V and E_C, (the gap between the band edges), the "damping constants" of the valence and conduction bands, γ_V and γ_C (gives the band tail width), the mass of the transition m (related to the strength of transition) and the decay factor f which drags down the imaginary part to zero at high frequencies (El-Amin and Solieman, 2015). In the OJL model, the refractive index n_f as a function of energy is

determined mainly by the parameter ‘mass’, which determines the shape of the conduction and valence band DOS. The empirical equations of DOS functions were adapted to include the transition in each of the DOS functions between the band region and the tail region. That is;

Density of state function for the valence band edge;

$$f_V(E)=\frac{\sqrt{2}m_v^{*\frac{1}{2}}}{\pi^2\hbar^3}\begin{cases}\sqrt{E_V-E} & \text{for } E \le E_V-\frac{1}{2}\gamma_V \\ \sqrt{\frac{1}{2}-\gamma_V}\ \exp\left(-\frac{1}{2}\right)\exp\left(\frac{E_V-E}{\gamma_V}\right) & \text{for } E > E_V-\frac{1}{2}\gamma_V\end{cases} \qquad (3.10)$$

Density of states for the conduction band edge;

$$f_C(E)=\frac{\sqrt{2}m_c^{*\frac{1}{2}}}{\pi^2\hbar^3}\begin{cases}\sqrt{E-E_C} & \text{for } E \ge E_C+\frac{1}{2}\gamma_C \\ \sqrt{\frac{1}{2}\gamma_C}\ \exp\left(-\frac{1}{2}\right)\exp\left(\frac{E-E_C}{\gamma_C}\right) & \text{for } E<E_C+\frac{1}{2}\gamma_C\end{cases} \qquad (3.11)$$

$f_V(E)$ and $f_C(E)$ are the density of states at the valence and conduction band respectively m_C^* and m_V^* are the effective masses of density of states at the conduction and valence band respectively. E_C and E_V denotes the sharp edges of conduction and valence bands, and γ_V and γ_C are the broadening spreads of valence band tail (VBT) and conduction band tail (CBT) states, respectively (El-Amin and Solieman, 2015).

The joint density of states (JDOS) function provides a measure of the number of allowed optical transitions between the occupied valence band electrons states and the unoccupied conduction band electronic states separated by a photon energy hv. The (JDOS) $J_{CV}(\hbar\omega)$

, associated with its broadened conduction and valence band is described by the following general equation (Saliba *et al.*, 2016).

$$J_{CV}(\hbar\omega) = \int_{-\infty}^{\infty} f_V(E)\, f_C(E+\hbar\omega)\, dE \tag{3.12}$$

The product of joint density of state and the oscillator strength yields the imaginary part of the dielectric function as described in equation 3.13;

$$\varepsilon_i(\hbar\omega) = (\pi e)^2 \left(\frac{4}{3\rho_A}\right) \xi^2(\hbar\omega)\, J_{CV}(\hbar\omega) \tag{3.13}$$

Where $\xi^2(\hbar\omega)$ is the normalized dipole matrix element and ρ_A the atomic density of material.

CHAPTER FOUR

MATERIALS AND METHODS

4.1 Synthesis of perovskite layers

In this study, two deposition methods were used for the formation of perovskite thin films. The methods were single step and double-step deposition methods. The glass slides which were commercially obtained were used as substrates where the perovskite thin films were deposited.

4.1.0 Substrate cleaning

The microscope slides, glass, 25x75 mm, 90^{o} ground edges, plain which were commercially purchased were used as the substrate were the perovskite thin films were deposited. Prior to their use the glass slides were cleaned to remove dirt and any residues from the surface. The glass slides were cleaned using bath of soapy water, a lint-free cotton swab was used to gently rub the surface clean. Rinsing was thoroughly done using deionized water and thereafter the glass slides were dried in air for 10 minutes.

4.1.1 Precursor solution preparation

In this study, ammonium salt in this case methyl ammonium iodide (MAI) which was whitish in color and metal halide; lead iodide (PbI_2) yellow in color both commercially purchased and in powder form were used without any alternation. Methyl ammonium iodide and lead iodide were mixed in the ration 1:1 and then dissolved in N, N- Dimethyl formamide (DMF) solution to come up with solution of different concentration. For instance 0.5g of methyl ammonium iodide powder was mixed with 0.5g of lead iodide and then dissolved in 10mL DMF to come up with solution of 0.05g/mL concentration. The

same procedure was used to obtain solution of 0.025g/mL, 0.0125g/mL and 0.00625g/mL of $CH_3NH_3PbI_3$ precursor solutions concentrations. The solutions were then subjected stirring condition at 60^oC for 30 minutes until a homogenous solution was obtained. This temperature was arrived at because it was found to be sufficient to make the solutes dissolve in the DMF. Precautionary measures such as wearing of gloves and face mask were made when handling DMF due to its toxic nature.

4.1.2 Single-Step solution deposition

Figure 4-0-1 shows perovskite solution being drop-casted on glass slide which acted as the substrate. The solution was drop-casted at the center of the glass substrate, and it spread out isotropically by applying the first law of Flick (Zhao *et al.*, 2014). There were four main key stages that were involved the formation of the perovskite film by single step namely; deposition of the solution in the substrate, spreading out of the solution in the substrate, evaporation of the excess solvent and finally film formation which resulted in dark-brown film in color.

The solution was then drop-casted on the glass substrates as illustrated in figure 4-0-1. The hot air sterilizer was used to evaporate the excess solvent from the substrate and the films were annealed at 80℃, 120℃ and 160℃ from the hot air sterilizer. These conditions led to different thin film morphologies as revealed by the micrographs obtained by the optical microscope.

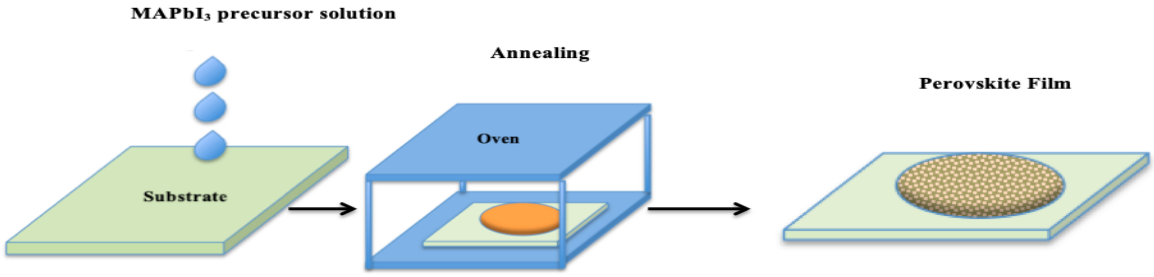

Figure 4-0-1 Illustration of single-step deposition of perovskite thin films

4.1.3 Double step solution deposition

This method has two steps: the first step involved formation of a layer of PbI_2 by drop casting a precursor solution of PbI_2 on to the preheated substrate as figure 4-0-2 illustrates. The PbI_2 solution was obtained by dissolving 1g of lead iodide powder in 100 ml of DMF. This solution was put under stirring condition in a hot plate at 60℃ to ensure that all solutes of PbI_2 dissolved. The solution was then drop-casted in glass slide and dried in a hot hair sterilizer at 120℃ for three minutes to remove the excess solvent. The double- step involved the dissolution of 0.5 g of methyl ammonium in 10 ml of propanol to give a solution of 0.05 g/mL concentration. The resulting films of PbI_2 were dipped in the solution of methyl ammonium and removed periodically at time intervals of 2 hours, starting with 2hours, 4 hours, 6 hours and finally 8 hours.

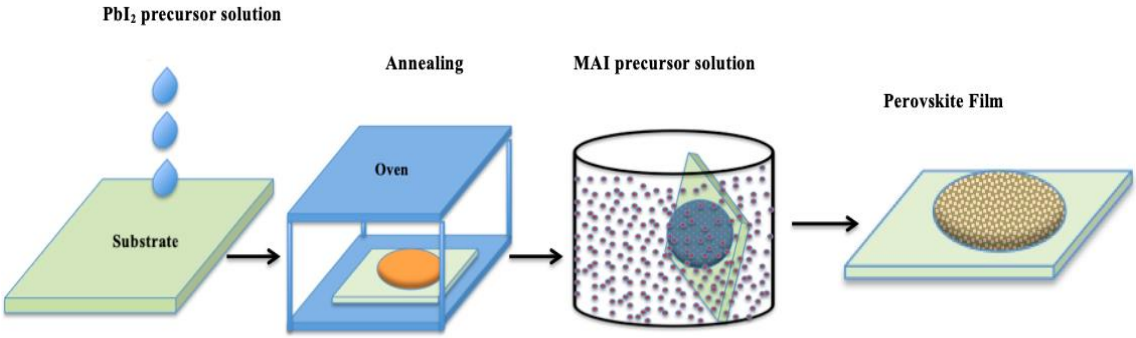

Figure 4-0-2 Illustration of double-step method for formation of perovskite thin films

4.2 Thin film characterization

4.2.0 UV-VIS optical characteristics

To compare the optical characteristics of the deposited perovskite layers, both the optical transmittance (*T*) and absorption (*A*) were measured in the wavelength range 300 -800 nm (*UV-VIS* range) on a computerized double beam spectrophotometer (Perkin Elmer Lambda 25). Using the experimentally obtained optical transmittance data from the spectrophotometer, this data was simulated using the SCOUT 4.06 software, where the following models were used; OJL model was used to obtain the optical band gap by use of the gap energy E_o, these values were divided by constant value 8085 and the results gave the band gap energy for films annealed at different temperatures and dipping times. The Drude model was used for optical constant analysis, where constants like absorption coefficient α, extinction coefficient k and refractive index n were directly obtained from the SCOUT software without any manipulation.

4.2.1 Optical microscopy

Optical microscopy (Motic digital Microscope) whose capture resolution was 2048x1536 pixels and digital resolution of 10 Mp-2592x1944 pixels connected to 240 voltage power source was used to map the morphology of the prepared organometallic halide perovskite thin films. The samples were used without any further modification. The objective lens was brought close to the sample being examined so that the light from the sample came to focus. Normal, photosensitive cameras captured the image from the optical microscope and a micrograph was generated.

4.3 Electrical characterization of the perovskite films

The resistivity of the films was determined by four point probe shown in the figure 4-0-3 below. All the four probes are aligned in a straight line as shown in figure 4-0-4. A calibrated constant source current of 4.53 mA was passed through the outer probes. Measurements were taken by pressing the four-point probe to the surface of the films. A source current was then activated and the sheet resistivity values displayed by the Keithley 2400 digital source measure unit (SMU).

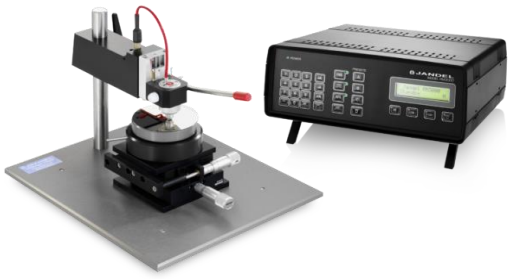

Figure 4-0-3 Four point probe

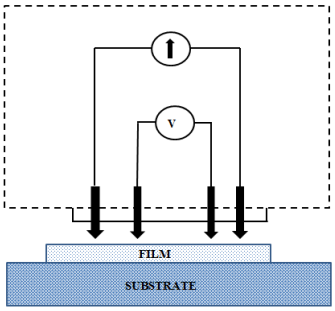

Figure 4-0-4 Illustration of four probes

Equation 4.1 was used to determine the sheet resistivity of the films

$$\rho_s = \frac{\rho}{d} \tag{4.1}$$

where, ρ_s = sheet resistivity, ρ = Resistivity, d = film thickness.

CHAPTER FIVE

RESULTS AND DISCUSSIONS

5.1 Introduction

The description of how optical transmittance (T), morphology, band gap energy (E_g), refractive index (η), absorption coefficient (α), extinction coefficient (k) and sheet resistivity ρ of perovskite films are affected by annealing temperature, concentration and dipping time will be done here.

5.2 Characterization of perovskite films deposited by Single-step method

5.2.1 Effects of concentration on the transmittance of perovskite films

Figure 5-0-1 shows the transmittance spectra of perovskite films with varying concentration. From the transmittance data, it was evident that transmittance of the films decreased with an increase in solution concentration. The films portrayed high transmittance in the visible region from 300nm-800nm. When the precursor solution concentration was 0.05 g/mL and 0.025 g/mL the prepared perovskite films had low transmittance as compared to the films with concentration of 0.0125g/ml and 0.00625 g/ml, annealed at the same temperature. This observation was attributed to; number of structures present and inter-structure distance as is evident from figure 5-0-4. When the precursor concentration was increased the number of structures present increased while the inter-structure distance decreased. Further an increase in concentration led to agglomeration of film structures meaning for higher concentration more particles diffused towards the growth front, thus through nucleation and crystallization processes they attached

themselves where there were maximum neighbors leading to agglomeration of film particles thus reducing the transmittance of the films obtained.

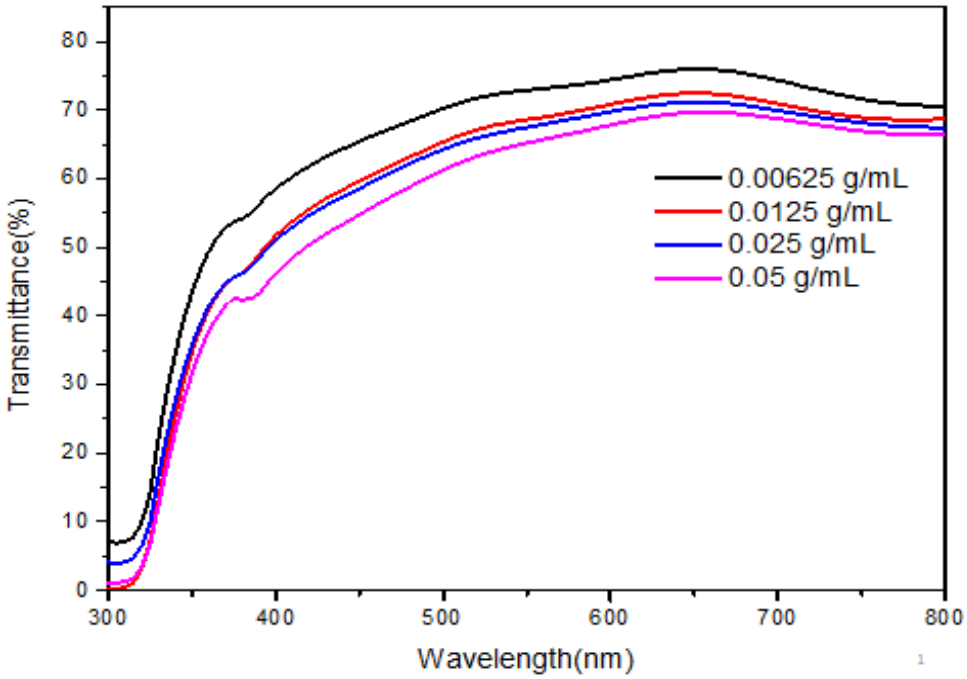

Figure 5-0-1Transmittance spectra for perovskite films with varying concentration

SCOUT modeling was used to obtain the band gap energy of the perovskite films as illustrated in figure 5-0-3. Considering the configuration of the semiconductor/ substrate system, OJL model was used to find the wavenumbers or gap energy E_o which when divided by constant value 8085 the band gap energy values were obtained. The drude model was used for optical constant analysis, where optical constants like refractive index n, extinction coefficient k and absorption coefficient α were obtained using the model. A best fit was obtained between the experimental data and the fitted transmittance. The

successful fitting processes of the deposited films were in agreement between the measured and fitted spectra as shown in figure 5-0-2 below.

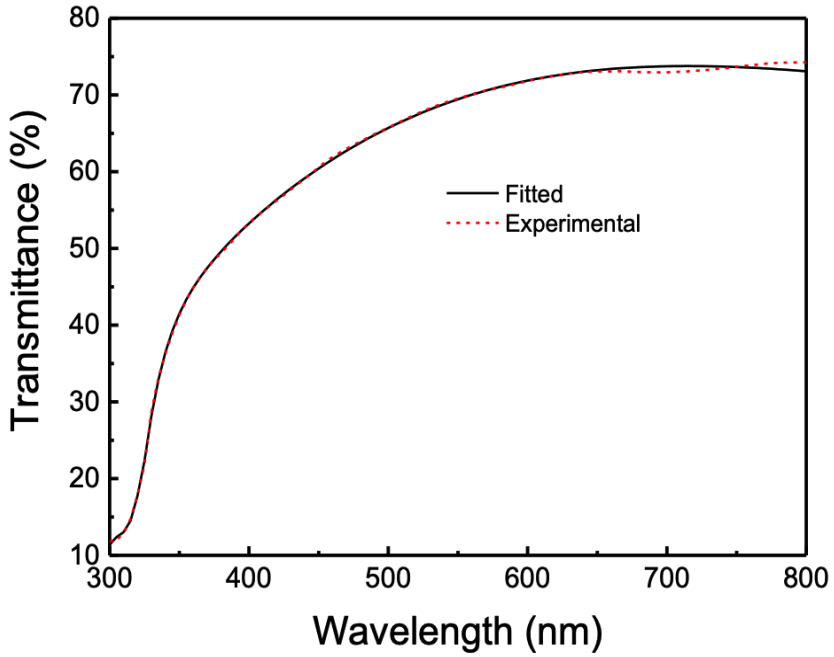

Figure 5-0-2 Experimental-fit transmittance spectra of perovskite thin film obtained using SCOUT software

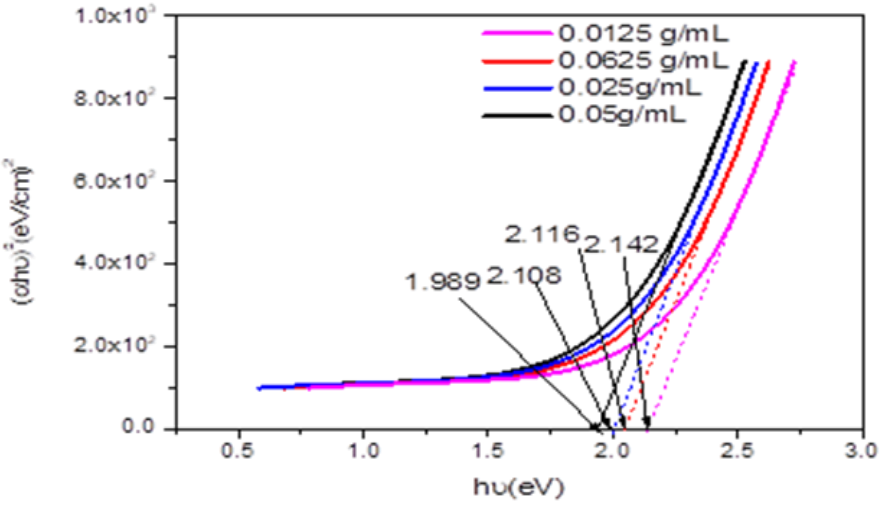

Figure 5-0-3 Band gap energy for perovskite films with varying concentrations

Figure 5-0-3 is shows the band gap energies for films annealed at the same temperature 160°C but having different concentration. The band gap decreased from 2.142eV to 1.989 eV. This result was supported by the fact that transmittance was observed to reduce as concentration of the solution was increased from 0.00625g/ml to 0.05g/ml and this signified the enhancement of optical properties of the methyl-ammonium lead iodide thin films ($MAPbI_3$).

The perovskite solar cell performance greatly depends on the morphology of the perovskite film (Saliba *et al.*, 2016). The deposition procedure to the great extent determines the kind of

morphology obtained as evidenced from the micrographs obtained by the two deposition methods. The number of structures for the considered concentrations reduced tremendously when concentration was reduced across as depicted in figure 5-0-4.

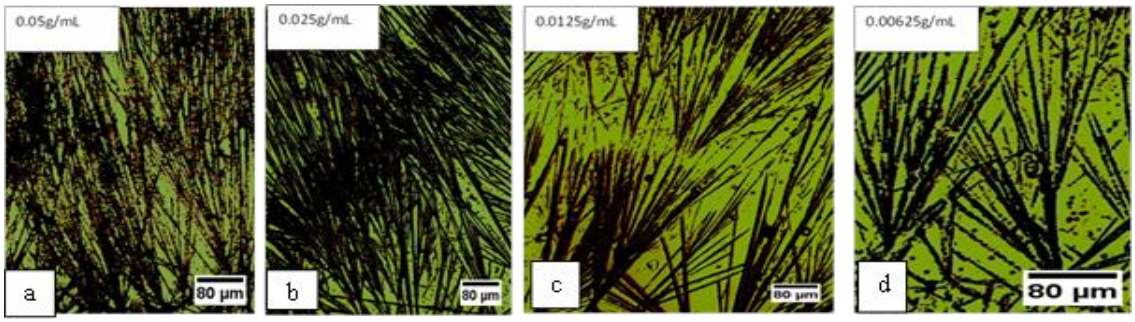

Figure 5-0-4 Optical micrographs of perovskite films with different concentrations

These perovskite films were annealed at 160°C, even though the film growth of the four considered concentrations that is 0.05g/mL 0.025g/mL, 0.0125g/mL and 0.00625g/mL is similar the only distinction is the number structures present and the inter-structure distance which reduced as the concentration was increased.

Micrograph with higher concentration that is figure 5-0-4 (a) exhibited high number of structures and reduced inter-structure distance as compared to the micrographs with lower concentration as depicted in figure 5-0-4 (d) that had the least structures this was for the simple reason that an increase in concentration increased the number of particles that diffused towards the growth front, for this reason there were many particles in the growth front for solution that had higher concentration as compared with the solution with lower concentartion . From the above observations it was deduced that concentration of a solution is key when depositing perovskite thin films, as this will alter the number of particles

present in the growth front and thus have direct impact on the structural growth and inter-structure distance and hence the surface morphology of the film.

5.2.2 Effects of temperature on the morphology of perovskite films

Figure 5-0-5 Optical micrographs for films annealed at different temperatures

Figure 5-0-5 shows micrographs that were obtained using the motic digital microscope. Form the micrographs it was observed that when the annealing temperature was increased from 80℃ to 160℃, the number of structures and nucleation centres reduced, the grain size and inter-grain distance increased. This was explained by the probability of attachment and detachment that came into play as the annealing was increased from 80℃ to 160℃ (Mwende, 2019). At 80℃ the probability of attachment is high and this meant that when the perovskite particle diffuses towards the growth front, it will take some time to examine the growth front and finally attach itself where there are maximum neighbours. At this annealing temperature the probability of attachment is higher as compared to the probability of detachment. This led to the growth of structures from many nucleation sites resulting into many structure, also other structures grew not only from the nucleus but also from the existing structures (spherulity structures).

At high temperatures of 160℃ the probability of detachment was very high as compared to the probability of attachment and this meant that a particle would take the shortest time to diffuse to the growth front but since the temperatures were very high it would attach and then detach itself until it gets suitable growth front where it will attach itself. Further at these high temperatures we had nucleation site coalesce and form single nucleus from which growth took place this resulted in the formation of single big grain sizes as illustrated in figure 5-0-5 (c). An increase in temperature beyond 160℃ resulted in the formation of yellow colour in the substrate indicating the presence of lead iodide on the substrate. Thus very high temperatures led to the decomposition of perovskite film. Film growth at low temperatures was characterized by many structures and presence of spherulitic structures which happens due to re-crystallization while at higher temperatures growth was characterized by single film growth and large spaces in between.

5.2.3 Effects of temperature on transmittance of perovskite films

As the annealing temperature was increased from 80℃ to 160℃ subsequently the transmittance of the $MAPbI_3$ film slightly reduced as illustrtated in figure 5-0-6 which indicated the enhancement of optical properties of the film after annealing. This meant that low temperatures were not sufficient to drive out the excess solvent as well as carrying out the growth process of perovskite. This was further supported by the fact that films annealed at room temperature demonstrated increased transmittance in the spectra. It was deduced that for perovskite film to form, two energy systems is required, one to remove the excess solvent and another one to carry out the growth process of methyl ammonium lead iodide. Thus low temperatures were found to be insufficient to carry out the growth process.

Temperatures above 160℃ were found not to be desirable for perovskite formation as they led to the decomposition of methyl ammonium, which resulted to the formation of yellow film on the substrate signalling presence of lead. Thus temperatures of 120℃ and 160℃ was recommended for annealing of perovskite film as this they were found to be ideal to carry out the two processes listed above. Thus temperature was found to be very important parameter when annealing perovskite films as the morphology of the resulting film greatly depended on the annealing temperature. Further the reduced transmittance at high annealing temperatures was associated with the formation of large crystalline islands that were associated with high temperatures.

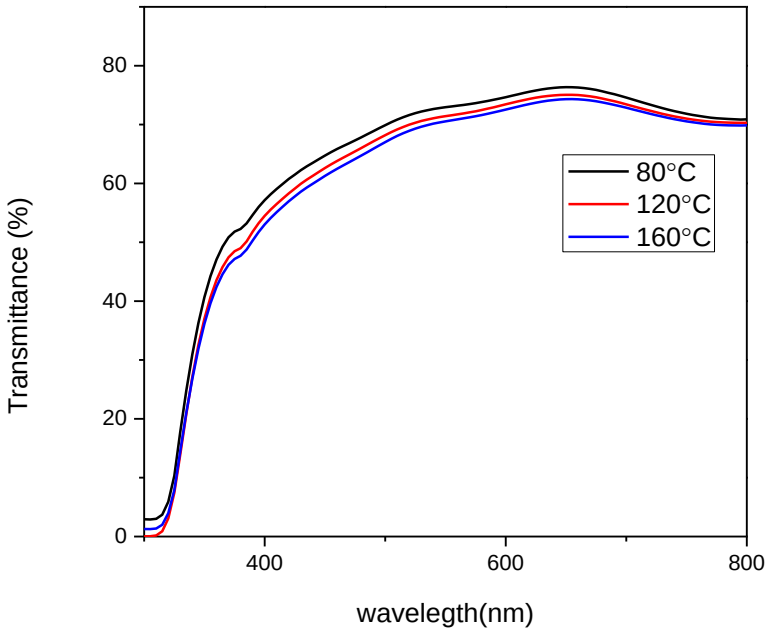

Figure 5-0-6 Transmittance for perovskite films annealed at different temperatures

Large grain sizes and ordering of molecules in the crystal contributed immensely to the reduction of the band gap of the perovskite films as the annealing temperature **was**

increased from 80℃ to 160℃ as illustrated in figure 5-0-7. Reduced band gap is the desired property for an excellent performance of PV devices for commercial consumption. This low optical band gap also increases the absorption range in semiconductor materials. These results were similar to the findings of Omondi, (2018) who found out that thermal annealing of $CH_3NH_3PbI_3$ films narrows the optical band gap energy.

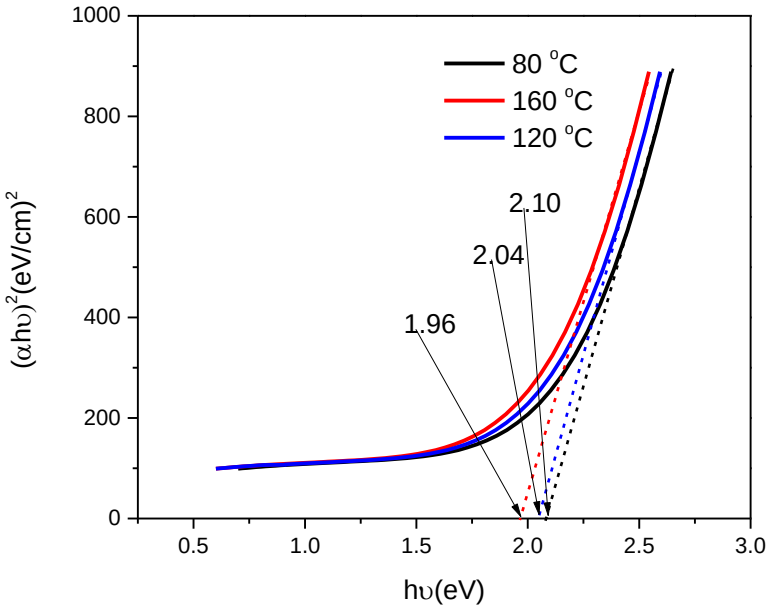

Figure 5-0-7 Band gap energy of perovskite films annealed at different temperatures

Electrical properties

The electrical resistivity of organometallic halide perovskites thin films decrease with an increase in the film thickness. This is explained using Petritz barrier model (Yaghoobi *et al.,* 2019). It has been demonstrated that annealing can have an effect on resistivity of $MAPbI_3$ films. Figure 5-0-8 show graph of sheet resistivity of the $MAPbI_3$ verses the

annealing temperature. It can be noted from graph that annealing temperature plays an important role in changing the sheet resistivity of the perovskite thin films.

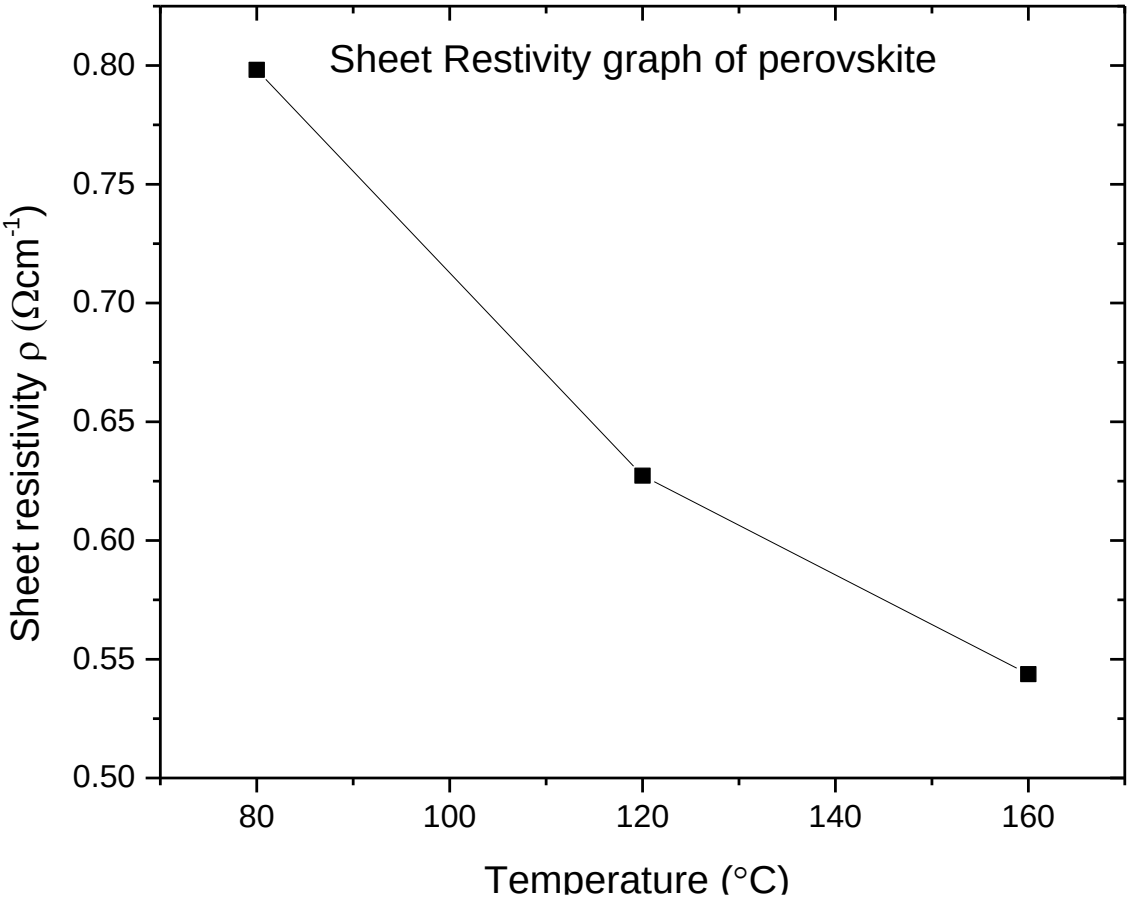

Figure 5-0-8 Effect of annealing temperatures on the sheet resistivity of perovskite films

When the annealing temperature was increased from 80℃ to 160℃, the sheet resistivity of the resulting perovskite film gradually decreased as shown in figure 5-0-8. This was attributed to factors like molecular ordering, increase in grain size ,reduced band gap, low transmittance of the films annealed at 160℃ arising from an increase of structural diameter

of the films necessitated by single, large crystalline growth, increased refractive index and absorption coefficient which were dependent on the high annealing temperatures of 160ºC. All these factors considered gave the films annealed at 160ºC better conducting properties hence reduced sheet resistivity.

5.3 Double-Step deposition

5.3.1 Effects of dipping time on optical properties on perovskite films

Transmittance reduced as dipping time was increased from 2 hours to 8 hours. In the UV-Vis range, the transmittance of the perovskite thin films decreased with an increase in the thickness of the thin films, which increased by lengthening the dipping time. An increase in film thickness leads to decrease in strain value, this can be attributed to inappropriate glass-film hence film layer adjacent to glass substrate will have some defects. As the film thickness increases the defects will slowly be suppressed (Mathew *et al.,* 2014). Figure 5-0-9 illustrates transmittance spectra for perovskite thin films deposited at varying deposition times. The films annealed after 8 hours demonstrated reduced transmittance in the entire spectral range as compared to the films that were annealed after 2, 4 and 6 hours. This was possible because the solutions were allowed enough time for crystallization and film growth to take place and form perovskite films with well-defined structures and shown micrographs in figure 5-0-11

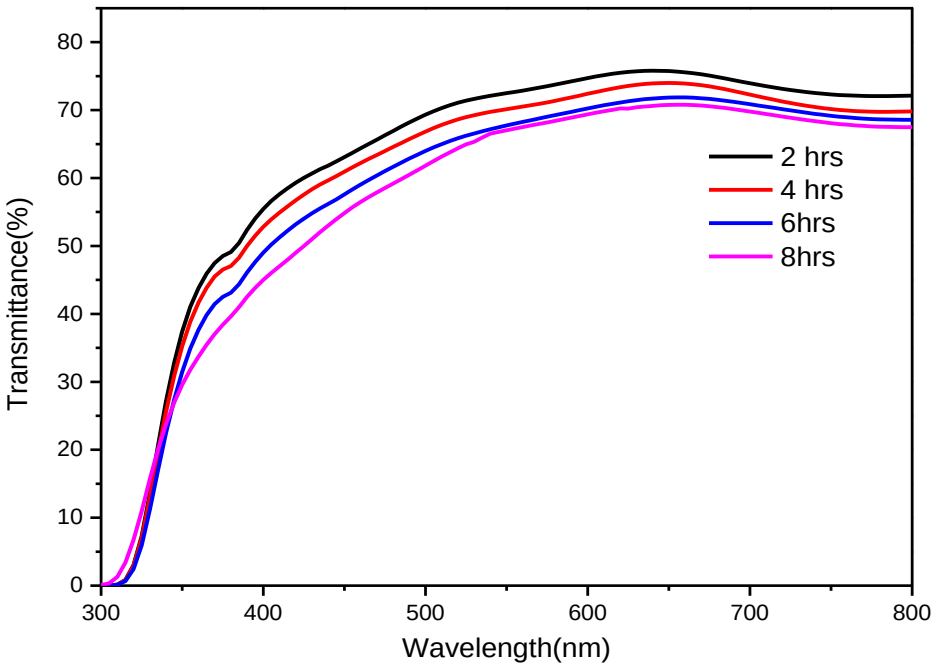

Figure 5-0-9 Transmittance spectra for perovskite thin films deposited at varying dipping times.

It can be seen from figure 5-0-10 that the band gap of perovskite reduced from 2.142 eV to 1.958 eV as the dipping time was increased from 2 hours to 8 hours respectively. Electrons move faster from valence band to conduction band when the band gap is narrower thus increasing conductivity. Reduced transmittance which implies increased absorbance, molecular ordering of the films, high refractive index, increased grain size and inter-grain distance of the resulting films obtained after 8 hours contributed immensely to the reduction of the band gap of the perovskite material. For maximum utilization in PV devices, reduced band gap is an excellent property. (Leyden *et al.*, 2014) used double step method to prepare perovskite films, where band gap energy of 1.59 eV was achieved.

These results were in close agreement with the results obtained by the researcher listed above.

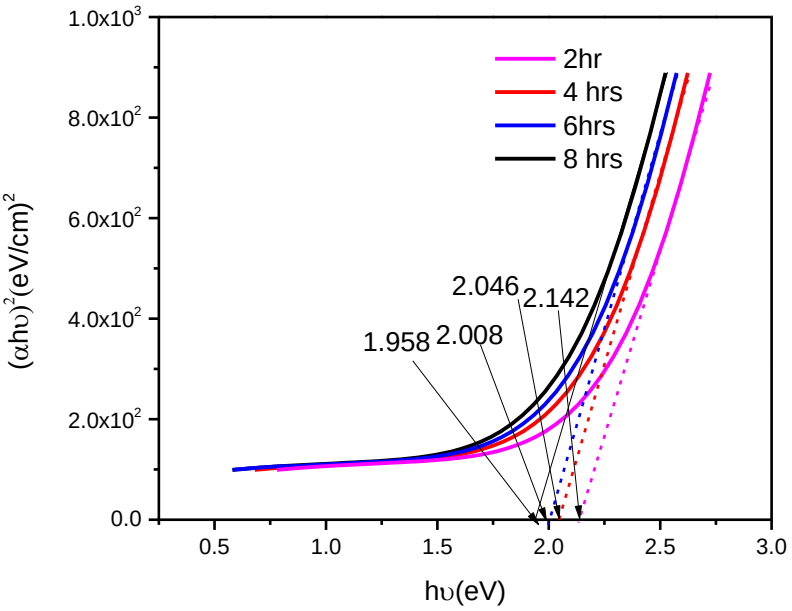

Figure 5-0-10 Band gap energy for double step method

Figure 5-0-11 shows morphology of perovskite thin films dipped at different deposition times. The sample deposited and annealed after 2 hours showed irregularly distributed needle-like shapes characterized by small grain sizes. This was due to the insufficient nucleation and film growth time, this being kinetic growth or time dependent film growth, the exposure time plays a major role in film formation and growth (-Mwende,2019). Thus for two hours it was realized that lead iodide and methyl ammonium iodide did not have enough time to diffuse towards the growth front carry, undergo nucleation process and finally grow to form perovskite films. While sample dipped and removed after 8 hours

demonstrated distinct and clear structures with large grain sizes as illustrated in figure 5-0-11 (d). This was attributed to the sufficient growth time that allowed for lead iodide and methyl ammonium iodide to crystallize and grow forming perovskite films. Further an increase in dipping time beyond 10 hours led to the decomposition of the lead iodide and nethyl ammonium iodide thus yellowish surface was observed when the substrate when it was observed by the optical microscope indicating presence of lead.

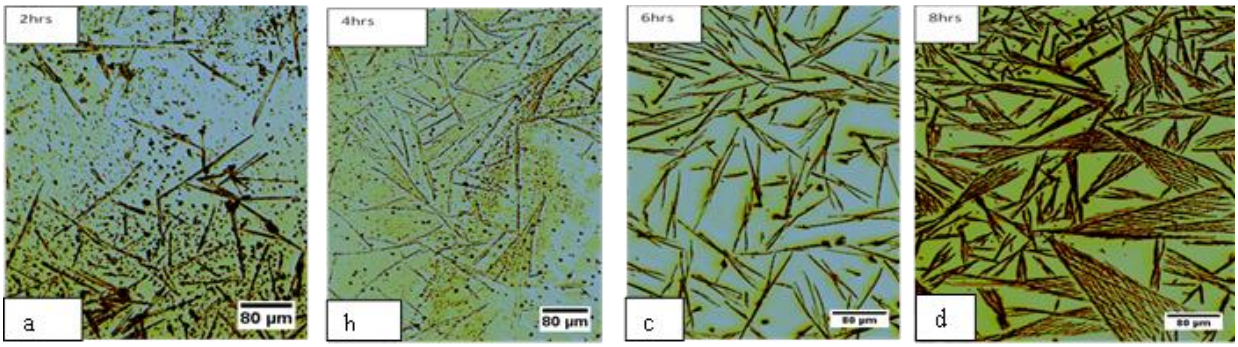

Figure 5-0-11 Optical micrographs for films dipped for (a) 2 hours, (b) 4 hours, (c) 6 hours and (d) 8 hours

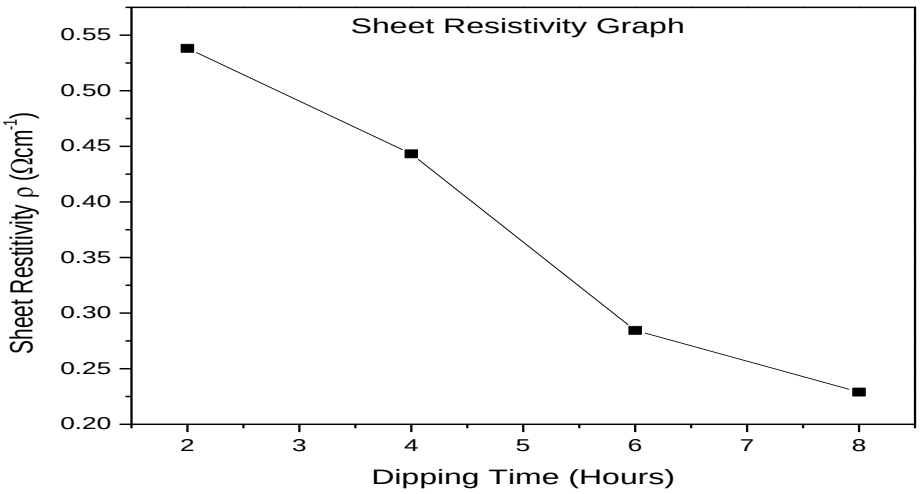

Figure 5-0-12 Influence of dipping time on electrical properties of perovskite film

The sheet resistivity of the perovskite films decreased as illustrated in figure 5-0-12 when the dipping time was increased from 2 hours to 8 hours. This was attributed to decreased band gap as the dipping time was increased from 2 to 8 hours. Further an increase in the grain sizes and reduced transmittance as the dipping time was increased contributed immensely to the decrease in the sheet resistivity.

CHAPTER SIX

CONCLUSIONS AND RECOMMENDATIONS

- The morphology of the perovskite films was found to be enhanced not only by the deposition method but also annealing temperature and dipping time
- An increase in both temperature and dipping time led to the production of well-defined and distinct structures of perovskite films and increase in grain size and demonstrated by the micrographs
- The films deposited and annealed by single step demonstrated both reduced band gap and sheet resistivity of 1.96eV and 0.5431 Ω cm^{-1} respectively.
- Films deposited by double step achieved a band gap of 1.95eV and sheet resistivity of 0.2290 Ω cm^{-1} .
- In summary temperature, concentration and annealing time were found to be fundamental factors in preparation of perovskite films, that is the film morphology of the films greatly depends on the above mentioned factors
- For future research, there is need to find suitable replacement of lead as it is considered poisonous.
- Further I recommend that the material be used for fabrication of solar cells to check on its power conversion efficiency.

REFERENCES

Andualem, A. and Demiss, S. (2018). Review on Dye - Sensitized Solar Cells (DSSCs). *Sci Tech*, 6.

Badescu, V. (2008). "Modeling Solar Radiation at the Earth's Surface." Springer Berlin Heidelberg, Berlin, Heidelberg.

Baines, T., Shalvey, T. P., and Major, J. D. (2018). CdTe Solar Cells. *In* "A Comprehensive Guide to Solar Energy Systems," pp215–232. Elsevier.

Bisquert, J. (2013). The Swift Surge of Perovskite Photovoltaics. *J. Phys. Chem. Lett.* **4**, 2597–2598.

Bost, M. C. and Mahan, J. E. (1988). An investigation of the optical constants and band gap of chromium disilicide. *J. Appl. Phys.* **63**, 839–844.

Brehm, J. A., Bennett, J. W., Schoenberg, M. R., Grinberg, I., and Rappe, A. M. (2014). The Structural Diversity of *AB* S $_3$ Compounds with d^0 Electronic Configuration for the *B* -Cation. *J. Chem. Phys.* **140**, 1–18.

Brittman, S., Adhyaksa, G. W. P., and Garnett, E. C. (2015). The expanding world of hybrid perovskites: materials properties and emerging applications. *MRS Commun.* **5**, 7–26.

Burschka, J., Pellet, N., Moon, S.-J., Humphry-Baker, R., Gao, P., Nazeeruddin, M. K., and Grätzel, M. (2013). Sequential deposition as a route to high-performance perovskite-sensitized solar cells. *Nature* **499**, 316–319.

Cabrera, C.I., solorio, D.A., and Hernandez, L. (2016). Joint density of states in low dimensional semiconductors. *Low dimensional systems and nanostructures* **76**, 103-108

Chawla, P. and Tripathi, M. (2015). Novel Improvements in the Sensitizers of Dye-Sensitized Solar Cells for Enhancement in Efficiency-A Review: Novel Sensitizers. *Int. J. Energy Res.* **39**, 1579–1596.

Chebrolu, V. T. and Kim, H.-J. (2019). Recent Progress in Quantum Dot Sensitized Solar Cells: An Inclusive Review of Photoanode, Sensitizer, Electrolyte, and the Counter Eemperature dependent transient surfaceelectrode. *J. Mater. Chem. C* **7**, 4911–4933.

Chopra, K. L., Paulson, P. D., and Dutta, V. (2004). Thin-film solar cells: an overview. *Prog. Photovolt. Res. Appl.* **12**, 69–92.

Christian, B.H., and Shamarr, B (2019). Absorption coefficient of semiconductor material *J. Appl. Phys.* **63**, 939–944.

Etgar, L., Gao, P., Xue, Z., Peng, Q., Chandarian, K., Liu, B., Nazeeruddin, K. and Gratzel, M.(2012). Mesoscopic $CH_3NH_3PbI_3/TiO_2$ herojunction solar cells. *Journal of the American Chemicals Society*, **134:** 17396-17399.

Etgar, D. A., Rappe, A. M., and Kronik, L. (2016). Hybrid Organic–Inorganic Perovskites on the Move. *Acc. Chem. Res.* **49**, 573–581.

El-Amin, A. A. and Solieman, A. (2015). Influence of Heat Treatment on the Optical Properties of Thermal Evaporated SnO2 Thin Films. *Silicon* **8**, 517–523.

Eperon, G. E., Stranks, S. D., Menelaou, C., Johnston, M. B., Herz, L. M., and Snaith, H. J. (2014). Formamidinium Lead Trihalide: A broadly Tunable Perovskite for Efficient Panar Heterojunction Solar Cells. *Energy Environ. Sci.* **7**, 982.

Espinosa, N., Serrano-Luján, L., Urbina, A., and Krebs, F. C. (2015). Solution and vapour deposited lead perovskite solar cells: Ecotoxicity from a life cycle assessment perspective. *Sol. Energy Mater. Sol. Cells* **137**, 303–310.

Fraas, L. M. (2014). History of Solar Cell Development. *In* "Low-Cost Solar Electric Power" (L.M. Fraas), pp1–12. Springer International Publishing, Cham.

Frost, J. M., Butler, K. T., Brivio, F., Hendon, C. H., Schilfgaarde, M. van, and Walsh, A. (2014). Atomistic Origins of High-Performance in Hybrid Halide Perovskite Solar Cells. *Nano Lett.* **14**, 2584–2590.

Fthenakis, V. M. and Kim, H. C. (2007). CdTe Photovoltaics: Life Cycle Environmental Profile and Comparisons. *Thin Solid Films* **515**, 5961–5963.

García-Valverde, R., Cherni, J. A., and Urbina, A. (2010). Life cycle analysis of organic photovoltaic technologies. *Prog. Photovolt. Res. Appl.* **18**, 535–558.

Green, M. A. (2009). The path to 25% silicon solar cell efficiency: History of silicon cell evolution. *Prog. Photovolt. Res. Appl.* **17**, 183–189.

Green, M. A., Dunlop, E. D., Hohl-Ebinger, J., Yoshita, M., Kopidakis, N., and Ho-Baillie, A. W. Y. (2020). Solar cell efficiency tables (Version 55). *Prog. Photovolt. Res. Appl.* **28**, 3–15.

Green, M. A., Emery, K., Hishikawa, Y., Warta, W., and Dunlop, E. D. (2015). Solar cell efficiency tables (Version 45): Solar cell efficiency tables. *Prog. Photovolt. Res. Appl.* **23**, 1–9.

Guinard, D., Grand, P. P., Bodereau, N., Cowache, P., Guillemoles, J.-F., Lincot, D., Taunier, S., Ben Farah, M., and Mogensen, P. (2002). Copper indium diselenide solar cells prepared by electrodeposition. *In* "Conference Record of the Twenty-Ninth IEEE Photovoltaic Specialists Conference, 2002.," pp692–695. IEEE, New Orleans, LA, USA.

Im, J.-H., Lee, C.-R., Lee, J.-W., Park, S.-W., and Park, N.-G. (2011). 6.5% efficient perovskite quantum-dot-sensitized solar cell. *Nanoscale* **3**, 4088.

Jackson, P., Hariskos, D., Lotter, E., Paetel, S., Wuerz, R., Menner, R., Wischmann, W., and Powalla, M. (2011). New World Record Efficiency for Cu(In,Ga)Se2 Thin-Film Solar Cells Beyond 20%. *Prog. Photovolt. Res. Appl.* **19**, 894–897.

Jena, A. K., Kulkarni, A., and Miyasaka, T. (2019). Halide Perovskite Photovoltaics: Background, Status, and Future Prospects. *Chem. Rev.* **119**, 3036–3103.

Jun, H. K., Careem, M. A., and Arof, A. K. (2013). Quantum dot-sensitized solar cells—perspective and recent developments: A review of Cd chalcogenide quantum dots as sensitizers. *Renew. Sustain. Energy Rev.* **22**, 148–167.

Kagan, C. R., Mitzi, D. B., and Dimitrakopoulos, C. D. (1999). Organic-Inorganic Hybrid Materials as Semiconducting Channels in Thin-Film Field-Effect Transistors. *Sci. New Ser.* **286**, 945–947.

Kamat, P. V. (2013). Evolution of Perovskite Photovoltaics and Decrease in Energy Payback Time. *J. Phys. Chem. Lett.* **4**, 3733–3734.

Lee, M. M., Teuscher, J., Miyasaka, T., Murakami, T. N., and Snaith, H. J. (2012). Efficient Hybrid Solar Cells Based on Meso-Superstructured Organometal Halide Perovskites. *Science* **338**, 643–647.

Leyden, M. R., Ono, L. K., Raga, S. R., Kato, Y., Wang, S., and Qi, Y. (2014). High performance perovskite solar cells by hybrid chemical vapor deposition. *J Mater Chem A* **2**, 18742–18745.

Liu, Y., Zhao, J., Li, Z., Mu, C., Ma, W., Hu, H., Jiang, K., Lin, H., Ade, H., and Yan, H. (2014). Aggregation and morphology control enables multiple cases of high-efficiency polymer solar cells. *Nat. Commun.* **5**, 5293.

Malinkiewicz, O., Yella, A., Lee, Y. H., Espallargas, G. M., Graetzel, M., Nazeeruddin, M. K., and Bolink, H. J. (2014). Perovskite solar cells employing organic charge-transport layers. *Nat. Photonics* **8**, 128–132.

Mathew, S., Yella, A., Gao, P., Humphry-Baker, R., Curchod, B. F. E., Ashari-Astani, N., Tavernelli, I., Rothlisberger, U., Nazeeruddin, Md. K., and Grätzel, M. (2014). Dye-Sensitized Solar Cells With 13% Efficiency Achieved Through the Molecular Engineering of Porphyrin Sensitizers. *Nat. Chem.* **6**, 242–247.

Michael, W.D and Mortimer, A. (2016). Polarized Light Microscopy - Microscope Configuration | Olympus LS (olympus-lifescience.com).

Mitzi, D. B., Chondroudis, K., and Kagan, C. R. (2001). Organic-inorganic electronics. *IBM J. Res. Dev.* **45**, 29–45.

Miyasaka, T., Teshima, K., Shirai, Y., and Kojima, A. (2009). Organometal Halide Perovskites as Visible-Light Sensitizers for Photovoltaic Cells. *J. Am. Chem. Soc.* **131**, 6050–6051.

Miyata, A., Mitioglu, A., Plochocka, P., Portugall, O., Wang, J. T.-W., Stranks, S. D., Snaith, H. J., and Nicholas, R. J. (2015). Direct measurement of the exciton binding energy and effective masses for charge carriers in organic–inorganic tri-halide perovskites. *Nat. Phys.* **11**, 582–587.

Mohan, R. and Paulose, R. (2019). Brief Review on Copper Indium Gallium Diselenide (CIGS) Solar Cells. *In* "Photoenergy and Thin Film Materials," pp157–192. John Wiley & Sons, Ltd.

Mwende. M (2019) Correlation Between the Preparation Methods and the Structural Morphologies of Organometallic Halide Perovskite Thin Films. **Thesis**

Omondi, C. A. (2018). Investigation of Hybrid Organic-Inorganic Lead Halide Perovskites by Modulated Surface Photovoltage Spectroscopy. **Thesis**.

O'Regan, B. and Gratzelt, M. (1991). A Low-Cost, High-Efficiency Solar Cell Based on Dye-Sensitized Colloidal TiO2 Films. **353**, 737–740.

Othman, A. R. and Rushdi, A. T. (2014). Potential of Building Integrated Photovoltaic Application on Roof Top of Residential Development in Shah Alam. *Procedia - Soc. Behav. Sci.* **153**, 491–500.

Pan, Z., Rao, H., Mora-Seró, I., Bisquert, J., and Zhong, X. (2018). Quantum dot-sensitized solar cells. *Chem. Soc. Rev.* **47**, 7659–7702.

Parisi, M. L., Maranghi, S., and Basosi, R. (2014). The evolution of the dye sensitized solar cells from Grätzel prototype to up-scaled solar applications: A life cycle assessment approach. *Renew. Sustain. Energy Rev.* **39**, 124–138.

Park, N.-G. (2015). Perovskite solar cells: an emerging photovoltaic technology. *Mater. Today* **18**, 65–72.

Park, N.-G. (2013). Organometal Perovskite Light Absorbers Toward a 20% Efficiency Low-Cost Solid-State Mesoscopic Solar Cell. *J. Phys. Chem. Lett.* **4**, 2423–2429.

Park, N.-G., Grätzel, M., Miyasaka, T., Zhu, K., and Emery, K. (2016). Towards stable and commercially available perovskite solar cells. *Nat. Energy* **1**, 16152.

Patwardhan, S., Cao, D. H., Hatch, S., Farha, O. K., Hupp, J. T., Kanatzidis, M. G., and Schatz, G. C. (2015). Introducing Perovskite Solar Cells to Undergraduates. *J. Phys. Chem. Lett.* **6**, 251–255.

Rao, S., Morankar, A., Verma, H., and Goswami, P. (2016). Emerging Photovoltaics: Organic, Copper Zinc Tin Sulphide, and Perovskite-Based Solar Cells. *J. Appl. Chem.* **2016**, 1–12.

Rathore, N., Panwar, N. L., Yettou, F., and Gama, A. (2019). A comprehensive review of different types of solar photovoltaic cells and their applications. *Int. J. Ambient Energy*, 1–18.

Saliba, M., Matsui, T., Seo, J.-Y., Domanski, K., Correa-Baena, J.-P., Nazeeruddin, M. K., Zakeeruddin, S. M., Tress, W., Abate, A., Hagfeldt, A., and Grätzel, M. (2016). Cesium-containing triple cation perovskite solar cells: improved stability, reproducibility and high efficiency. *Energy Environ. Sci.* **9**, 1989–1997.

Snaith, H. J. (2013). Perovskites: The Emergence of a New Era for Low-Cost, High-Efficiency Solar Cells. *J. Phys. Chem. Lett.* **4**, 3623–3630.

Urbach, F. (1953). The Long-Wavelength Edge of Photographic Sensitivity and of the Electronic Absorption of Solids. *Phys. Rev.* **92**, 1324–1324.

Wehrenfennig, C., Liu, M., Snaith, H. J., Johnston, M. B., and Herz, L. M. (2014). Charge-carrier dynamics in vapour-deposited films of the organolead halide perovskite $CH_3NH_3PbI_{3-x}Cl_x$. *Energy Env. Sci* **7**, 2269–2275.

Wu, X. (2004). High-Efficiency Polycrystalline CdTe Thin-Film Solar Cells. *Sol. Energy* **77**, 803–814.

Yaghoobi Nia, N., Lamanna, E., Zendehdel, M., Palma, A. L., Zurlo, F., Castriotta, L. A., and Di Carlo, A. (2019). Doping Strategy for Efficient and Stable Triple Cation Hybrid Perovskite Solar Cells and Module Based on Poly(3-hexylthiophene) Hole Transport Layer. *Small* **15**, 1–10.

Yan, J. and Saunders, B. R. (2014). Third-generation solar cells: a review and comparison of polymer:fullerene, hybrid polymer and perovskite solar cells. *RSC Adv* **4**, 43286–43314.

Yin, W.-J., Shi, T., and Yan, Y. (2014). Unique Properties of Halide Perovskites as Possible Origins of the Superior Solar Cell Performance. *Adv. Mater.* **26**, 4653–4658.

Zhang, Y., Stokes, N., Jia, B., Fan, S., and Gu, M. (2015). Towards ultra-thin plasmonic silicon wafer solar cells with minimized efficiency loss. *Sci. Rep.* **4**, 4939.

Zhao, Y. and Zhu, K. (2014). Solution Chemistry Engineering toward High-Efficiency Perovskite Solar Cells. *J. Phys. Chem. Lett.* **5**, 4175–4186.

Ziang, X., Shifeng, L., Laixiang, Q., Shuping, P., Wei, W., Yu, Y., Li, Y., Zhijian, C., Shufeng, W., Honglin, D., Minghui, Y., and Qin, G. G. (2015). Refractive index and extinction coefficient of CH_3NH_3PbI_3 studied by spectroscopic ellipsometry. *Opt. Mater. Express* **5**, 29.

APPINDIX

UV-VIS spectrophotometer used for obtaining transmittance of the perovskite thin films (Chiromo Campus- University of Nairobi)

Image of optical microscope connected with laptop for imaging of films

Hot air sterilizer used to dry the films

Image of four point probe used to measure the sheet resistivity of thin films